

Removal of Batch Effects using Distribution-Matching Residual Networks

Uri Shaham^{1*}, Kelly P. Stanton^{2,3*}, Jun Zhao⁴, Huamin Li³, Ruth Montgomery⁵,
and Yuval Kluger^{2,3}

November 26, 2022

¹Department of Statistics, Yale University, New Haven, CT, USA

²Department of Pathology, Yale School of Medicine, New Haven, CT, USA

³Applied Mathematics Program, Yale University, New Haven, CT, USA

⁴Program in Computational Biology and Bioinformatics, Yale University, New Haven, CT, USA

⁵Department of Internal Medicine, Yale School of Medicine, New Haven, CT, USA

Abstract

Sources of variability in experimentally derived data include measurement error in addition to the physical phenomena of interest. This measurement error is a combination of systematic components, originating from the measuring instrument, and random measurement errors. Several novel biological technologies, such as mass cytometry and single-cell RNA-seq, are plagued with systematic errors that may severely affect statistical analysis if the data is not properly calibrated. Here, we propose a novel deep learning approach for removing systematic batch effects. Our method is based on a residual network, trained to minimize the Maximum Mean Discrepancy (MMD) between the multivariate distributions of two replicates, measured in different batches. We apply our method to mass cytometry and single-cell RNA-seq datasets, and demonstrate that it effectively attenuates batch effects, and outperforms several popular methods.

1 Introduction

Biological data are affected by the conditions of the measuring instruments. For example, biomedical data from replicated¹ measurements, measured in different batches, may be distributed differently due to variation in these conditions between batches. The term *batch effects*, often used in the biological community, describes a situation where subsets (batches) of the measurements significantly differ in distribution, due to irrelevant instrument-related factors (Leek et al., 2010). Batch effects introduce systematic error, which may cause statistical analysis to produce spurious results and/or obfuscate the signal of interest.

*The first two authors contributed equally to this work.

¹We use the term *replicates* to refer to technical replicates, i.e., multiple measurements of the same specimen, for example, two blood drops of the same person.

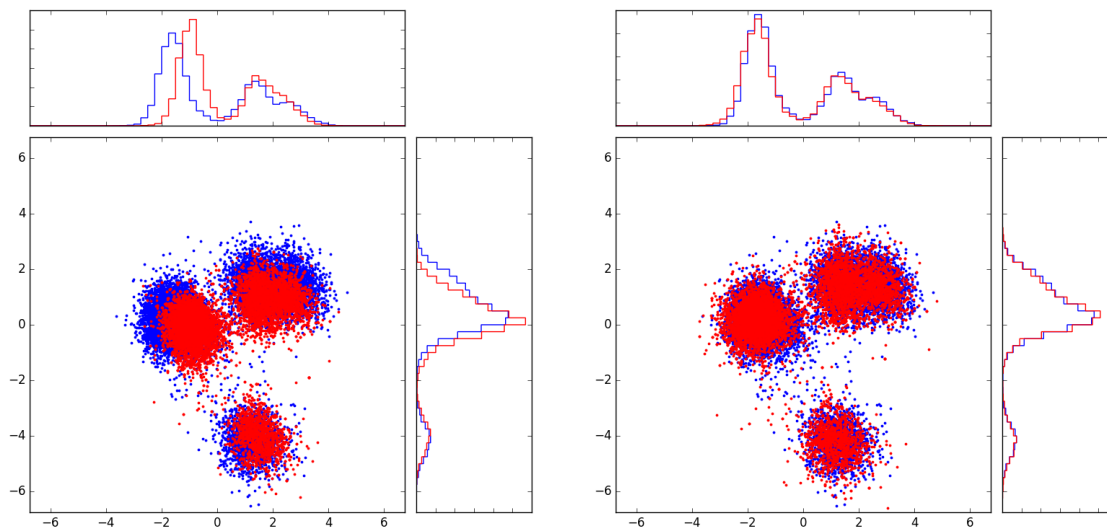


Figure 1: Calibration of CyTOF data: projection of the source and target test samples on the first two principal components of the target data. Left: before calibration. Right: after calibration. For better visualization, only cells with known cell types are plotted.

For example, CyTOF, a mass cytometry technique for measuring multiple protein levels in many cells of a biological specimen, is known to incur batch effects. When replicate blood specimens from the same patient are measured on a CyTOF machine in different batches (e.g. different days), they might differ noticeably in the distribution of cells in the multivariate protein space. In order to run a valid and effective statistical analysis on the data, a calibration process has to be carried out, to account for the effect of the difference in instrument conditions on the measurements.

Typically, the systematic effect of varying instrument conditions on the measurements depends on many unknown factors, whose impact on the difference between the observed and underlying true signal cannot be modeled. In this manuscript, we consider cases where replicates differ in distribution, due to batch effects. By designating one replicate to be the source sample² and the other to be the target sample, we propose a deep learning approach to learn a map that calibrates the distribution of the source sample to match that of the target. Our proposed approach is designed for data where the difference between these source and target distributions is moderate, so that the map that calibrates them is close to the identity map; such an assumption is fairly realistic in many situations. An example of the problem and the output of our proposed method is depicted in Figure 1. A short demo movie is available at <https://www.youtube.com/watch?v=Lqya9WDkZ60>.

Furthermore, we empirically show that a map from a source batch to a target batch, learned

²The term *sample* is used with different meanings in the biological and statistical communities. Both meanings are used in this manuscript, however, usage should be clear from context. .

using two replicate samples prepared/extracted from the same specimen, to which we refer as a reference, can be used to map additional samples from the source batch to the target batch. Generalizing this approach allows one to calibrate multiple source batches to a single target batch, where a reference replicate is measured in each of these batches. Revisiting the CyTOF example, suppose that in each day we run the instrument to measure blood of a several (different) individuals, and in addition we also measure in each of these runs a replicate of the reference blood sample. Training our proposed net at each day t on the corresponding replicate of the reference blood sample, it learns a map ψ_t that calibrates the measurements from day t to have the same distribution as the reference replicate at day 0. While ψ_t is learned solely from the reference replicates, it can then be used to calibrate data of other patients that were also measured at day t . This way data from all days may be compared, by mapping all samples to coordinates of day 0.

The remainder of this manuscript is organized as follows: in Section 2 we give a brief review of Maximum Mean Discrepancy and Residual Nets, on which our approach is based. The calibration learning problem is defined in Section 3, where we also describe our proposed approach. Experimental results on CyTOF and RNA-seq measurements are reported in Section 4. In Section 5 we review some related works. The manuscript concludes with a discussion in Section 6.

2 Preliminaries

2.1 Maximum Mean Discrepancy

Maximum Mean Discrepancy (MMD, Gretton et al. (2012, 2006)) is a measure for distance between two probability distributions p, q . It is defined with respect to a function class \mathcal{F} by

$$\text{MMD}(\mathcal{F}, p, q) \equiv \sup_{f \in \mathcal{F}} (\mathbb{E}_{x \sim p} f(x) - \mathbb{E}_{x \sim q} f(x)). \quad (1)$$

When \mathcal{F} is a reproducing kernel Hilbert space with kernel k , the MMD can be written as the distance between the mean embeddings of p and q

$$\text{MMD}^2(\mathcal{F}, p, q) = \|\mu_p - \mu_q\|_{\mathcal{F}}^2, \quad (2)$$

where $\mu_p(t) = \mathbb{E}_{x \sim p} k(x, t)$. Equation (2) can be written as

$$\begin{aligned} \text{MMD}^2(\mathcal{F}, p, q) &= \mathbb{E}_{x, x' \sim p} k(x, x') - 2\mathbb{E}_{x \sim p, y \sim q} k(x, y) \\ &\quad + \mathbb{E}_{y, y' \sim q} k(y, y'), \end{aligned} \quad (3)$$

where x and x' are independent, and so are y and y' . Importantly, if k is a universal kernel, then $\text{MMD}(\mathcal{F}, p, q) = 0$ iff $p = q$. In practice, the distributions p, q are unknown, and instead we are given observations $\{x_1, \dots, x_n\}, \{y_1, \dots, y_m\}$, so that the (biased) sample version of (3)

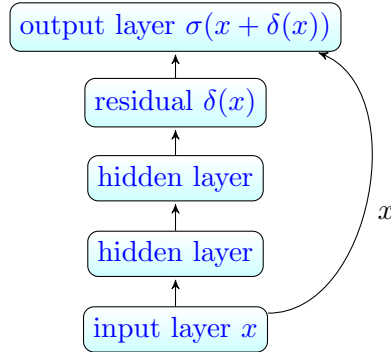


Figure 2: A ResNet block. ResNets typically contain a sequence of such blocks, where the hidden layers usually perform convolutions, followed by non-linearity and pooling. σ is an element-wise nonlinear activation function, e.g. ReLU.

becomes

$$\begin{aligned} \text{MMD}^2(\mathcal{F}, X, Y) &= \frac{1}{n^2} \sum_{x_i, x_j \in X} k(x_i, x_j) \\ &\quad - \frac{2}{nm} \sum_{x_i \in X, y_j \in Y} k(x_i, y_j) \\ &\quad + \frac{1}{m^2} \sum_{y_i, y_j \in Y} k(y_i, y_j). \end{aligned}$$

MMD was originally proposed as a non-parametric two sample test, and has since been widely used in various applications. Li et al. (2015); Dziugaite et al. (2015), use it as a loss function for neural net; here we adopt this direction to tackle the calibration problem, as discussed in Section 3.

2.2 Residual Nets

Residual neural networks (ResNets, He et al. (2015)) is a recently introduced technique for training very deep networks, mostly used for image recognition tasks. ResNets can formed by concatenation of many blocks, where each block has a form similar to Figure 2. Each block receives input x (the output of the previous block) and computes output $y = \sigma(x + \delta(x))$, where σ is a non-linearity activation (typically ReLU) and $\delta(x)$ is the activation of the last layer of a small neural net. In other words, a block is a small neural net with a shortcut connection, which adds the input and the last layer.

Since a ResNets block consists of a residual term and an identity term, it can easily learn functions close to the identity function. This makes the optimization of very deep networks simpler and more successful than similar nets that do not have shortcut connections, as having

parts of the net learn near-identity functions from random initialization without constraints is significantly more difficult. It was empirically shown by He et al. (2015) that the performance of very deep convolutional nets without shortcut connections deteriorates beyond some depth, while ResNets can grow very deep with increasing performance.

Here, we adopt the framework of ResNet blocks for the task of calibration between replicate samples whose multivariate distributions are close to each other. To calibrate the samples, we are therefore interested in learning a map which is close to the identity map; a ResNet block structure is a convenient tool to learn such a map.

3 Tackling the Calibration Problem

Formally, we consider the following learning problem: let $\mathcal{D}_1, \mathcal{D}_2$ be two distributions on \mathbb{R}^d , such that there exists a continuous map $\psi : \mathbb{R}^d \rightarrow \mathbb{R}^d$ so that if $X \sim \mathcal{D}_1$ then $\psi(X) \sim \mathcal{D}_2$. We also assume that ψ is a small perturbation of the identity map.

We are given two finite samples $\{x_1, \dots, x_n\}, \{y_1, \dots, y_m\}$ from $\mathcal{D}_1, \mathcal{D}_2$, respectively. The goal is to learn a map $\hat{\psi} : \mathbb{R}^d \rightarrow \mathbb{R}^d$ so that $\{\hat{\psi}(x_1), \dots, \hat{\psi}(x_n)\}$ is likely to be a sample from \mathcal{D}_2 .

Since we assume that ψ is close to the identity, it is convenient to express it as $\psi(x) = x + \delta(x)$, where $\delta(x)$ is small, so that the connection to ResNets blocks becomes apparent.

Our proposed solution, which we term MMD-ResNet is a single ResNet block. The network gets two samples $\{x_1, \dots, x_n\}, \{y_1, \dots, y_m\}$ of points in \mathbb{R}^d . We refer to $\{x_1, \dots, x_n\}$ as the source sample and to $\{y_1, \dots, y_m\}$ as the target sample. The net is trained to learn a map of the source sample, to make it similar in distribution to the target sample. Specifically, we train the net with the following loss function

$$L(w) = \sqrt{\text{MMD}^2(\{\hat{\psi}(x_1), \dots, \hat{\psi}(x_n)\}, \{y_1, \dots, y_m\})},$$

where $\hat{\psi}$ is the map computed by the network, and depends on the network parameters w . We train the net in a stochastic mode, so that in fact the MMD is computed only on mini-batches from both samples, and not on the entire samples.

4 Experimental Results

In this section we report experimental results on biological data obtained using two types of high-throughput technologies: CyTOF and single-cell RNA-seq (scRNA-seq). CyTOF is a mass cytometry technology that allows simultaneous measurements of multiple protein markers in each cell of a specimen (e.g., a blood sample), consisting of $10^4 - 10^6$ cells (Spitzer and Nolan, 2016). scRNA-seq is a sequencing technology that allows to simultaneously measure mRNA expression levels of all genes in thousands of single cells.

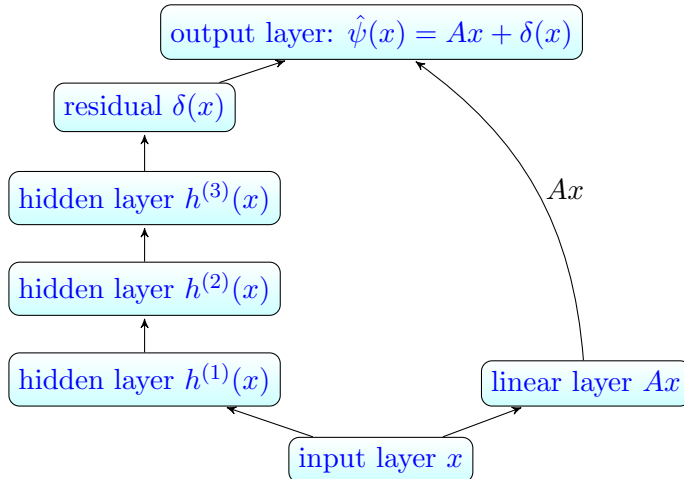


Figure 3: The net architecture used in our experiments.

4.1 Technical Details

As a standard practice, in each experiment the data was standardized so that each marker had zero mean and unit variance. All our experiments are done using a network with four hidden layers with ReLU units. Experimentally, we found that the network’s performance is improved by adding more flexibility to it, so that the shortcut connection passes a matrix multiplication Ax of the input x , where A is learned during training. The exact architecture we used is depicted in Figure 3. We initialized the net to compute the identity map, by initializing A to be the identity matrix and initializing the weights to zero, so that $\delta(x) = 0$. We observed slightly worse results when replacing the zero initialization by a standard initialization, e.g., Xavier (Glorot and Bengio, 2010).

For each pair of samples, we trained the net using one of the samples as source and the other as target. The net was trained using Adam (Kingma and Ba, 2014) and dropout (Srivastava et al., 2014). We used mini-batches of size 1000 from both the source and target samples. A subset 10% of the training data was held out for validation, to determine when to stop the training. We implemented our net in Keras; our codes will be made publicly available.

The kernel we used is a sum of three Gaussian kernels

$$k(x, y) = \sum_i \exp\left(-\frac{\|x - y\|^2}{\sigma_i^2}\right).$$

We chose the σ_i s to be $\frac{m}{2}, m, 2m$, where m is the median of the average distance between a point in the target sample to its nearest 20 neighbors.

4.2 Calibration of CyTOF Data

Mass cytometry uses a set of antibodies, each of which is conjugated to a unique heavy ion and binds to a different cellular protein. Cells are then individually nebulized and subjected to mass spectrometry. Protein abundance is indirectly observed from the signal intensity at each protein’s associated ions’ mass to charge ratio. Multiple specimens can be run in the same batch by using barcoding with additional ions to record the origin of each specimen (Spitzer and Nolan, 2016).

A CyTOF batch contains measurements of numerous cells from a few specimens, and each batch is affected by systematic errors (Finck et al., 2013). The experiments reported in this manuscript were performed on two replicate blood samples, drawn from a single patient and measured on different instruments as part of a multi-institute study (Nasaar et al., 2015). The two samples contained 27,715 and 26,105 cells respectively. Each of the two samples contained 26 markers, out of which eight correspond to the following immune cell lineage protein markers: CCR6, CD20, CD45, CD14, CD16, CD8, CD3, CD4; we perform our calibration experiments on this 8-dimensional data. The data was manually filtered by a human expert to remove debris and dead cells. In addition, a bead-normalization procedure was applied to the data; this is a current practice for normalizing CyTOF data (Finck et al., 2013). Yet, our results demonstrate that the samples clearly differ in distribution, despite the fact that they were normalized.

4.2.1 Calibrating Two Replicates

In this section we report the results of applying our proposed MMD-ResNet to calibrating two replicate samples, where we arbitrarily designated one as “source” and the other as “target”. The term “before calibration” refers to the source sample, while “after calibration” refers to the mapping of that sample, obtained from the net after training.

A multi-marker distribution of cells from CyTOF data tends to concentrate in several clusters corresponding to different cell types. We observed that the proportions of cell types detected in different CyTOF instruments vary. We therefore sub-sampled the source sample so that the relative proportion of each cell type in the sample would match the corresponding proportion in the target sample (see details in Section 6).

The projection of the target and source data onto the first two PCs of the target sample is shown in Figure 1. In the top plot, it is apparent that before calibration, the source sample (red) differs in distribution from the target sample (blue). After calibration (bottom plot), the gap between the source and the target distributions decreases significantly.

Figure 4 shows the empirical cumulative distribution functions of six of the eight markers in the source sample before and after the calibration, in comparison to the target sample. The remaining two markers are shown in Appendix A, due to space limitation. In all cases, the calibrated source curves resemble the corresponding target sample curves.

On a multivariate level, we compute the 8×8 correlation matrix of the source sample and subtract it from the correlation matrix of the target sample. If the source and target distributions are close, we expect the difference to be small. Figure 5 shows the resulting matrices before and after the calibration; clearly, the difference between the correlation matrices

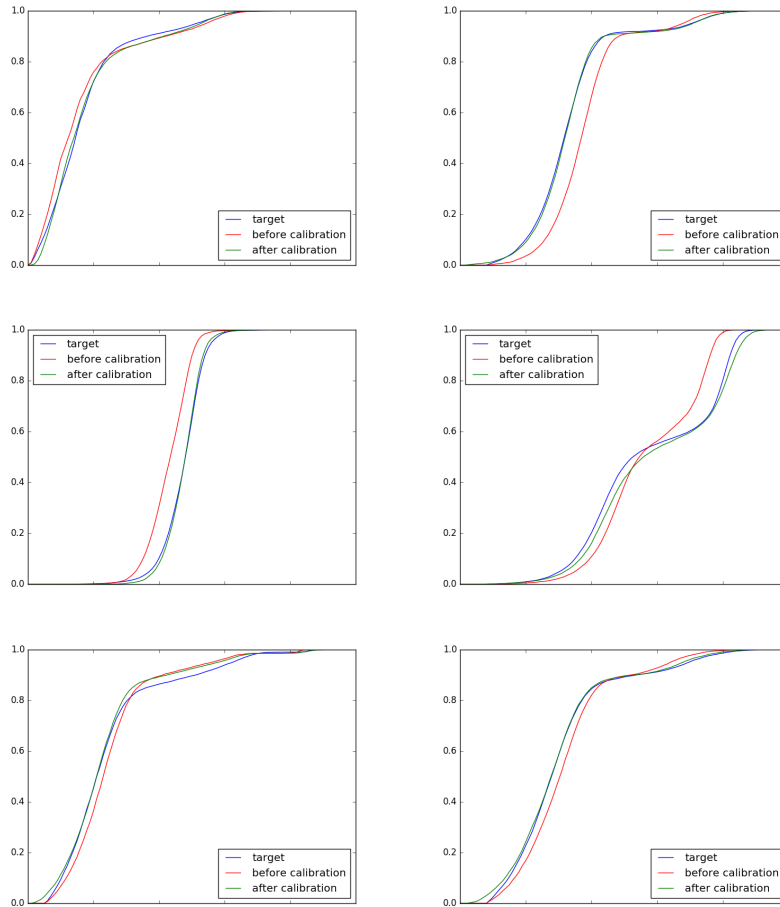


Figure 4: Empirical cumulative distribution functions of six of the 8 markers in the 10-14 experiment. In each plot the blue, red and green curves corresponds to the target, source and calibrated source samples, respectively. In each marker the blue and green curves are closer than the blue and red curves. Plots of the remaining two markers are presented in the appendix, due to space limitations.

is closer to zero after the calibration. Indeed, the Frobenius norm of the difference is 0.75 before the calibration, and 0.33 after the it. We remark that the fact that the norm decreases after the calibration implies that the data cannot be fully calibrated using linear transformation of each marker independently (e.g., z-transform), as the correlation of a single marker is invariant to such transformation. Hence, to tackle the calibration problem, a more comprehensive approach is needed than simply shifting and re-scaling single markers.

In addition, we also use MMD to measure the distance between the target and source distributions, before and after calibration. To do that, we sample several random batches of

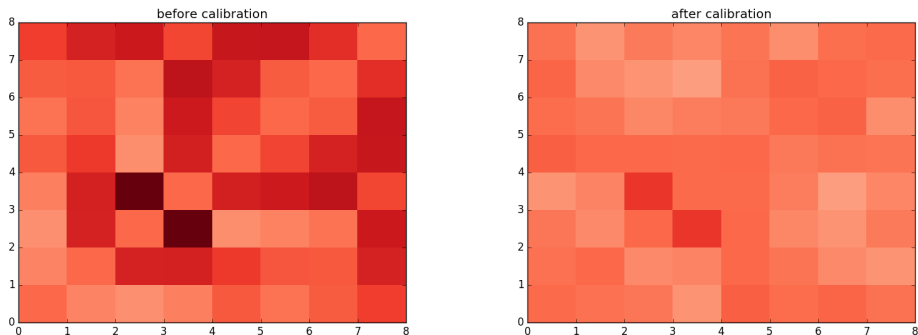


Figure 5: Differences between the correlation matrix of the target and source samples. Left: before calibration. Right: after calibration. After calibration the difference is smaller, implying that the MMD net captures the covariance structure in the target sample.

Table 1: MMD values between random batches of size 1000 from the source sample before and after calibration and target sample, using a Gaussian kernel with various scales. The MMD between two random batches of the target sample is provided as reference at the bottom row. At the three largest scales, the calibrated data is significantly closer in MMD to the target sample. The scales (σ_i 's) that were used during training are: 0.65, 1.31, and 2.62.

MMD \ scale	0.3	1	3	10
(before,target)	0.046	0.121	0.206	0.110
(after,target)	0.046	0.053	0.51	0.028
(target,target)	0.044	0.044	0.043	0.018

size 1000 from each of the distributions, and measure the MMD statistic using a Gaussian kernel with various scales. We compare the results to the MMD between two random batches from the target distribution. The results, shown in Table 1, demonstrate that the calibrated source is significantly closer in MMD to the target sample.

Finally, we compared the performance of the MMD-ResNet to two popular linear methods for calibration. The results, provided in Appendix B show that MMD-ResNet outperforms these two linear methods.

4.2.2 Generalizing to Unseen Samples

We now turn to the following question: Suppose we trained a MMD residual net to calibrate two replicated samples, say, one measured on instrument A and the other on instrument B . To what extent the network can also be used to calibrate measurements of other samples (possibly with different biological conditions) that were measured on instrument A to their corresponding values on instrument B ? Using a network, trained on replicated samples from

Table 2: MMD Calibration of two simulated patients through two nets. Despite that fact each net was trained on a single sample, it achieves equally good calibration on the other sample, which corresponds to a different density.

calib. by net \ patient	1	2
None	0.377	0.431
\mathcal{N}_1	0.143	0.155
\mathcal{N}_2	0.147	0.156

a reference specimen (e.g., a reference patient), to calibrate samples from different specimens would mean that this net is appropriate to account for batch effects. Clearly, one cannot guarantee good calibration in general on unseen samples, for example, in case that the densities of the two samples obtained from measurements using instrument A have disjoint supports. However, such a scenario is not plausible biologically. A more plausible scenario is that while the densities may differ, their supports nearly overlap. Under such conditions, we may hope to achieve good calibration of samples that were not presented to the network during training.

To empirically test this, we simulated replicate data of two patients, each patient measured on (the same) two instruments, using the following procedure: We first trained an MMD-ResNet \mathcal{N} to calibrate two replicate samples from our collection, as in Section 4.2.1. Denote the source sample by S , and assume it was subjected to measurements in instrument A . Let h be the vector of proportions of the major five sub-populations of cell types in S . We obtained two permutations h_1, h_2 of h and generated two new samples S_1, S_2 by re-sampling from S using the corresponding proportions vectors. As a result, the distributions of S_1, S_2 differ in density, but share the same support. To obtain the target samples, we calibrated S_1 and S_2 using \mathcal{N} . Denote the calibrated samples by T_1 and T_2 . We then trained a MMD residual net \mathcal{N}_1 on the pair (S_1, T_1) and a second net \mathcal{N}_2 on the pair (S_2, T_2) . S_1, T_1 therefore simulate samples of patient 1 taken on instrument A and B , and similarly S_2, T_2 simulate samples of patient 2, possibly with different biological conditions, on the same two instruments.

Finally, we check whether \mathcal{N}_1 can also calibrate S_2 , by comparing the calibration to the one that is performed by \mathcal{N}_2 . Table 2 shows the results of this simulated experiment. The fact that the second and third rows are similar implies that the MMD between calibrated S_1 and T_1 is similar, regardless of the network through which it is calibrated; similar pattern occurs with S_2 . This means that under the conditions in this experiment (i.e., different samples have different densities with similar supports), one can use a single net, trained on replicated samples from a reference patient that were measured on two instruments, to calibrate samples from new patients.

4.3 Calibration of single-cell RNA-seq data

Drop-seq (Macosko et al., 2015) is a novel technique for simultaneous measurement of single-cell mRNA expression levels of all genes of numerous individual cells. Unlike traditional single cell

sequencing methods, which can only sequence up to hundreds or a few thousands of cells (Picelli et al., 2013), (Jaitin et al., 2014) drop-seq enables researchers to analyze many thousands of cells in parallel, thus offers a better understanding of complex cell types of cellular states.

However, even with several thousands of cells (~ 5000) in each run, only less than half of the cells typically contain enough transcribed genes, that can be used for statistical analysis. As the number of cells in a single run is not sufficient for studying very complicated tissues; one needs to perform multiple runs, in several batches so that the cumulative number of cells is a good representation of the distribution of cell populations. This process may create batch effects, which need to be removed.

In (Macosko et al., 2015), seven batches were sequenced to study cell sub-types of mouse retina. The data contains 49,300 cells, 13,155 of which that express more than 900 genes were retained for further analysis. 384 genes with the largest variance were retained to explore the sub-population structure of the cells. Due to the nature of scRNA-seq, e.g., low depth and high dropout rate, the data matrix is very sparse. In our experiments below, we used a low rank approximation, so that actual zeros become non-zeros. Macosko et al. (2015) estimated that most of the signal is captured by the leading 32 principal components and used them for downstream analysis. We adopted their preprocessing steps and performed a calibration between batches using the 32-rank approximation of the $13,155 \times 384$ matrix.

We arbitrarily chose one of the batches to be the target batch and trained six MMD-ResNets, each net using one of the other six batches as a source batch. Figure 6 shows the projection of the batches onto the 19th and 21st principal components of the entire data, which are the two that are the most correlated with the target batch indicator vector (i.e., the directions where the target batch has the largest deviation from the other batches). In addition, we also plot the result of calibration using Combat (Johnson et al., 2007), a standard toolbox for batch effect removal in expression data, which was recently used to remove batch effects in scRNA-seq data (Shekhar et al., 2016). For clarity, only three of the batches are plotted. Plots containing all seven batches are presented in Appendix C. As can be seen, the source distribution is significantly closer to the target distribution after calibration using MMD-ResNet. Furthermore, the quality of calibration using MMD-ResNet is higher than the one performed by Combat.

5 Related Work

Leek et al. (2010) thoroughly discuss the importance of tackling batch effects and review several existing approaches for doing so.

Bead normalization (Finck et al., 2013) is a specific normalization procedure for CyTOF. As we observed in Section 4, two CyTOF samples may significantly differ in distribution even after Bead normalization. Warping (Hahne et al., 2010) is an approach for calibration of cytometry data where for each marker, the peaks of the marginal distribution in the source sample are (possibly non-linearly) shifted to match the peaks of the corresponding marginal in the target sample. We argue that warping can perhaps be performed by training MMD-ResNet for each single marker. The advantage of MMD-ResNet over a warping is that the former is multivariate,

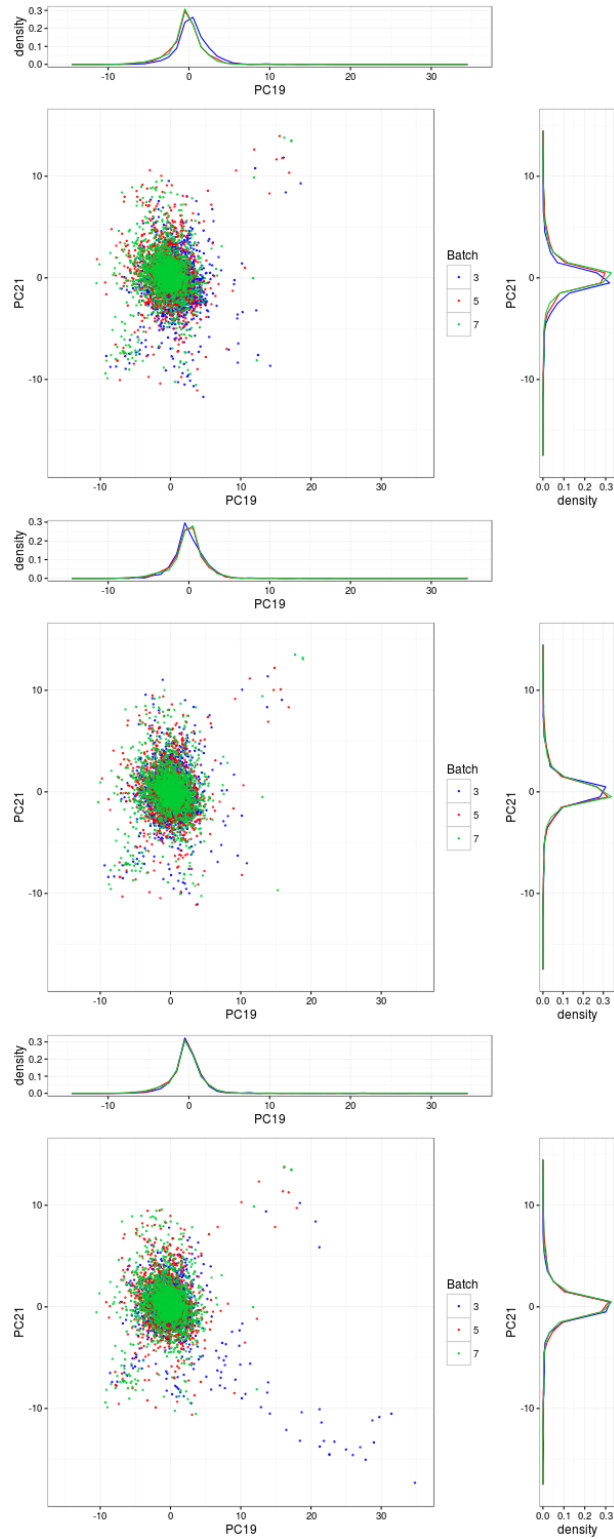


Figure 6: RNA-seq experiments. The plots show projection of the data onto the two principal components which are most correlated with the batch indicator vector. Top: before calibration. Center: calibration using Combat. Bottom: calibration using MMD-ResNet.

and can take into account dependencies, while the latter assumes that the joint distributions is a product of its marginals (Finak et al., 2014).

Surrogate variable Analysis (Leek and Storey, 2007) is a popular approach for batch effect adjustment, primarily in gene expression data. However, it is designed for inference scenarios, where there is a response variable that is to be predicted from the data, hence does not directly apply to our case, which is purely unsupervised.

MMD networks were proposed in (Li et al., 2015; Dziugaite et al., 2015) where the goal was to learn a generative model that can transform standard input distributions (e.g. white noise) to a target distribution. This line of work is closely related to the application presented in this manuscript. To the best of our knowledge, MMD nets have not been applied to the problem of removal of batch effects, which is considered here.

6 Discussion

Several issues need to be kept in mind while using MMD-ResNets for calibration. First, many recent works proposing generative models use Parzen window estimates for model evaluation. As Theis et al. (2015) nicely point out, evaluation of generative models using Parzen windows is problematic; in our context, for example, suppose that the net maps the source points to the centers of mass of the target sample. Such a map will have high Parzen likelihood estimates, while clearly not calibrating the data well. MMD, which takes also into account the internal structure of the calibrated source sample (term which is missing in Parzen estimates) might be a more suitable for evaluation of the quality of the calibration.

Second, we found out that identifying cluster structure of the data might be a useful practice prior to applying MMD-ResNets in certain applications. For instance, when one uses CyTOF to characterize peripheral blood mononuclear cells (PBMCs), the multi-marker cell distributions typically have separable clusters, corresponding to cell type sub-populations. While the relative proportion of different cell types in two replicate blood samples is expected to be invariant to the CyTOF machine, measuring these samples in two different runs in the same instrument or two different instruments often show noticeable differences between the cell type composition. When the proportions of corresponding clusters differ between the source and target distributions, we do not expect that MMD-ResNet will account for that difference, as it computes a continuous map. In the CyTOF experiments presented here, we sub-sampled the source dataset so that the proportion of each cell type will be the same in the source and target samples.

Lastly, despite the impressive experimental results presented here, a two sample test (say, a permutation test using MMD as a test statistic) will reject the hypothesis that the calibrated source sample has the same distribution as the target sample. Yet, in the same way that general deep learning techniques, operating on raw data outperform traditional algorithms tailored for specific data types and involve domain knowledge and massive pre-processing, we find our proposed approach and experimental results very promising and hope that they open new directions for removing batch effects in biological datasets. For example, recent proposed experimental approaches to standardization (Kleinstauber et al., 2016), should provide an excellent source for application of MMD-ResNet.

References

- Dziugaite, G. K., Roy, D. M., and Ghahramani, Z. (2015). Training generative neural networks via maximum mean discrepancy optimization. *arXiv preprint arXiv:1505.03906*.
- Finak, G., Jiang, W., Krouse, K., Wei, C., Sanz, I., Phippard, D., Asare, A., Rosa, S. C., Self, S., and Gottardo, R. (2014). High-throughput flow cytometry data normalization for clinical trials. *Cytometry Part A*, 85(3):277–286.
- Finck, R., Simonds, E. F., Jager, A., Krishnaswamy, S., Sachs, K., Fantl, W., Pe’er, D., Nolan, G. P., and Bendall, S. C. (2013). Normalization of mass cytometry data with bead standards. *Cytometry Part A*, 83(5):483–494.
- Glorot, X. and Bengio, Y. (2010). Understanding the difficulty of training deep feedforward neural networks. In *Aistats*, volume 9, pages 249–256.
- Gretton, A., Borgwardt, K. M., Rasch, M., Schölkopf, B., and Smola, A. J. (2006). A kernel method for the two-sample-problem. In *Advances in neural information processing systems*, pages 513–520.
- Gretton, A., Borgwardt, K. M., Rasch, M. J., Schölkopf, B., and Smola, A. (2012). A kernel two-sample test. *Journal of Machine Learning Research*, 13(Mar):723–773.
- Hahne, F., Khodabakhshi, A. H., Bashashati, A., Wong, C.-J., Gascoyne, R. D., Weng, A. P., Seyfert-Margolis, V., Bourcier, K., Asare, A., Lumley, T., et al. (2010). Per-channel basis normalization methods for flow cytometry data. *Cytometry Part A*, 77(2):121–131.
- Hastie, T., Tibshirani, R., Narasimhan, B., Chu, G., and Tibshirani, M. R. (2015). Package pamr.
- He, K., Zhang, X., Ren, S., and Sun, J. (2015). Deep residual learning for image recognition. *arXiv preprint arXiv:1512.03385*.
- Jaitin, D. A., Kenigsberg, E., Keren-Shaul, H., Elefant, N., Paul, F., Zaretsky, I., Mildner, A., Cohen, N., Jung, S., Tanay, A., et al. (2014). Massively parallel single-cell rna-seq for marker-free decomposition of tissues into cell types. *Science*, 343(6172):776–779.
- Johnson, W. E., Li, C., and Rabinovic, A. (2007). Adjusting batch effects in microarray expression data using empirical bayes methods. *Biostatistics*, 8(1):118–127.
- Kingma, D. and Ba, J. (2014). Adam: A method for stochastic optimization. *arXiv preprint arXiv:1412.6980*.
- Kleinsteuber, K., Corleis, B., Rashidi, N., Nchinda, N., Lisanti, A., Cho, J. L., Medoff, B. D., Kwon, D., and Walker, B. D. (2016). Standardization and quality control for high-dimensional mass cytometry studies of human samples. *Cytometry Part A*.

- Leek, J. T., Scharpf, R. B., Bravo, H. C., Simcha, D., Langmead, B., Johnson, W. E., Geman, D., Baggerly, K., and Irizarry, R. A. (2010). Tackling the widespread and critical impact of batch effects in high-throughput data. *Nature Reviews Genetics*, 11(10):733–739.
- Leek, J. T. and Storey, J. D. (2007). Capturing heterogeneity in gene expression studies by surrogate variable analysis. *PLoS Genet*, 3(9):e161.
- Li, Y., Swersky, K., and Zemel, R. (2015). Generative moment matching networks. In *International Conference on Machine Learning*, pages 1718–1727.
- Liu, Q. and Markatou, M. (2016). Evaluation of methods in removing batch effects on rna-seq data. *Infectious Diseases and Translational Medicine*, 2(1):3–9.
- Macosko, E. Z., Basu, A., Satija, R., Nemesh, J., Shekhar, K., Goldman, M., Tirosh, I., Bialas, A. R., Kamitaki, N., Martersteck, E. M., et al. (2015). Highly parallel genome-wide expression profiling of individual cells using nanoliter droplets. *Cell*, 161(5):1202–1214.
- Nasaar, A., Carter, B., Lannigan, J., Montgomery, R., Paul, N., Poulin, M., Raddassi, K., Rahman, A., and Rashidi, N. (2015). The first multi-center comparative study using a novel technology mass cytometry time-of-flight mass spectrometer (cytof2) for high-speed acquisition of highly multi-parametric single cell data: A status report. Presented at the 30th Congress of the International Society of Advancement of Cytometry.
- Nygaard, V., Rødland, E. A., and Hovig, E. (2016). Methods that remove batch effects while retaining group differences may lead to exaggerated confidence in downstream analyses. *Biostatistics*, 17(1):29–39.
- Picelli, S., Björklund, Å. K., Faridani, O. R., Sagasser, S., Winberg, G., and Sandberg, R. (2013). Smart-seq2 for sensitive full-length transcriptome profiling in single cells. *Nature methods*, 10(11):1096–1098.
- Shekhar, K., Lapan, S. W., Whitney, I. E., Tran, N. M., Macosko, E. Z., Kowalczyk, M., Adiconis, X., Levin, J. Z., Nemesh, J., Goldman, M., et al. (2016). Comprehensive classification of retinal bipolar neurons by single-cell transcriptomics. *Cell*, 166(5):1308–1323.
- Spitzer, M. H. and Nolan, G. P. (2016). Mass cytometry: Single cells, many features. *Cell*, 165(4):780–791.
- Srivastava, N., Hinton, G. E., Krizhevsky, A., Sutskever, I., and Salakhutdinov, R. (2014). Dropout: a simple way to prevent neural networks from overfitting. *Journal of Machine Learning Research*, 15(1):1929–1958.
- Theis, L., Oord, A. v. d., and Bethge, M. (2015). A note on the evaluation of generative models. *arXiv preprint arXiv:1511.01844*.

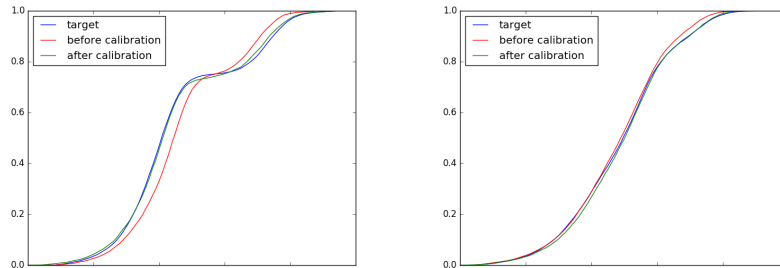


Figure 7: Empirical CDF of the two remaining markers which are not shown in Figure 4.

Table 3: MMD Comparison of calibration using (1) z -transform of each marker, (2) PCA and (3) ResNet. The table entries are MMD between the target sample and the calibrated source sample.

method \ scale	0.3	1	3	10
Z-transform	0.046	0.070	0.075	0.022
PCA	0.047	0.117	0.163	0.073
MMD-ResNet	0.046	0.053	0.051	0.028
(target,target)	0.044	0.045	0.040	0.018

A The Two Remaining Markers in the CyTOF Experiment

See Figure 7.

B Comparison to Linear methods

In this section we compare the quality of calibration of our net to two of the most popular techniques for removal of batch effects. The simplest and most common (Nygaard et al., 2016) adjustment is zero centering, i.e., subtracting from any value the global mean of its batch; see, for example the *batchadjust* command in the R package PAMR (Hastie et al., 2015). Here we compare the performance of the net to the calibration that is achieved by matching each marker’s mean and variance in the source sample to the corresponding values in target sample.

The second common practice is to obtain the principal components of the data, and removing the components that are most correlated with the batch index (Liu and Markatou, 2016). Table 3 shows the MMD between the source and target samples in each approach. As can be seen, the calibration obtained from our MMD-ResNet outperforms the ones obtained by the methods mentioned above. Figure 8 shows plots comparing MMD-ResNet calibration with the above to methods. The per-marker linear calibration discards much of the calibration effect, yet the calibration achieved by the net looks better.

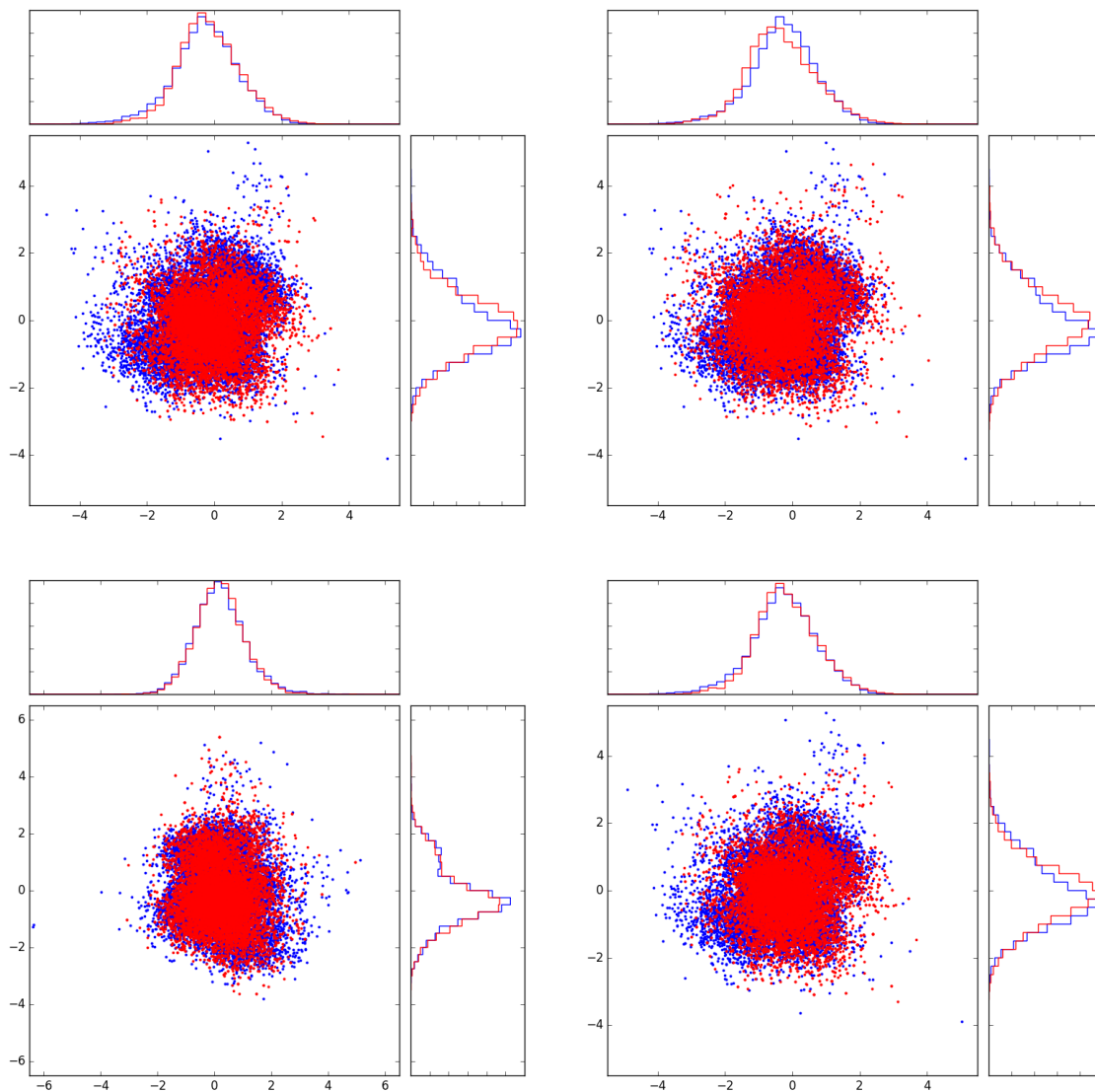


Figure 8: Comparison between calibration using MMD-ResNet and two linear methods. Each plot shows projection onto the subspace of the fourth and fifth principal components of the target data. From top left, clock-wise: before calibration, calibration using z -transform of each marker, calibration by removing the principal component most correlated with the batch, nonlinear calibration using MMD-ResNet.

C Additional Plots from the RNA experiment

See Figure 9.

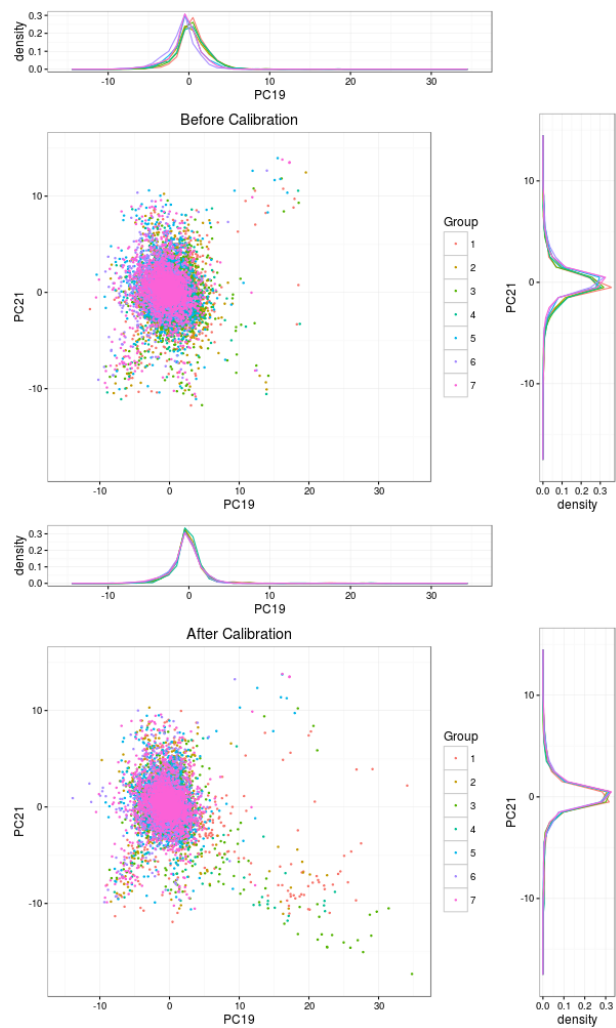


Figure 9: Additional plots scRNA-seq experiments. The plots show all seven batches, projected onto the first two principal components of the data. Top: before calibration. Bottom: after calibration with MMD-ResNet.